Surface & Coatings Technology 378 (2019) 124915

Contents lists available at ScienceDirect

Surface & Coatings Technology

journal homepage: www.elsevier.com/locate/surfcoat

High temperature interaction of volcanic ashes with 7YSZ TBC's produced by APS: Infiltration behavior and phase stability

Marco A. Rivera-Gil[a], Juan J. Gomez-Chavez[b], C.V. Ramana[b], Ravisankar Naraparaju[c], Uwe Schulz[c], Juan Muñoz-Saldaña[a,*]

[a] Laboratorio Nacional de Proyección Térmica (CENAPROT), Centro de Investigación y de Estudios Avanzados del IPN, Libramiento Norponiente 2000, Fracc. Real de Juriquilla, 76230 Querétaro, Mexico
[b] Department of Mechanical Engineering, University of Texas at El Paso, El Paso, TX 79968, USA
[c] Institute of Materials Research, German Aerospace Center, Cologne 51147, Germany

ARTICLE INFO

Keywords:
TBC
Atmospheric plasma spray
YSZ
Volcanic ashes
Infiltration
High temperature

ABSTRACT

High-temperature infiltration behavior and phase stability of yttria-stabilized zirconia (7YSZ) thermal barrier coatings (TBC) produced by atmospheric plasma spray interacting with volcanic ashes (VAs) are presented here. Three VAs from the Colima, Popocatepetl, and Eyjafjallajökull volcanoes have been used in this work. Previous to infiltration experiments, physicochemical characterization of the VAs was carried out including thermal analyses by DSC, structural studies by XRD, and ICP chemical composition measurements. TBCs' infiltration tests were carried out at 1250 °C for different times. Results showed that infiltration depth as a function of time behaves in a non-linear way. Mainly two important infiltration behaviors were identified corresponding to high- and slow-speed infiltration regimes. Higher infiltration kinetics was detected for VAs with lower SiO_2 content. The extent of chemical degradation of the 7YSZ is directly related to the silica content. For greater SiO_2 values, a higher content of monoclinic ZrO_2 was observed leading to maximum values at intermediate annealing times between 2 and 5 h. This behavior can be correlated with the high-speed tetragonal to monoclinic ZrO_2 transformation at short times (between 2 and 5 h) until a maximum monoclinic content is reached. After that, the reaction follows by the interplay of $ZrSiO_4$ formation at the expense of previously formed *m*-ZrO_2 together with the incorporation of Y and Zr to the glass melt.

1. Introduction

The development of today's turbine engines used in the aeronautic industry has been the result of relentless efforts dedicated to achieving an increase in efficiency and operational safety of aeronautical propulsion systems. Such efficiency increments are related to the engine's operating temperature increase acquired thanks to advances in materials science. Among design materials, thermal barrier coatings (TBCs) have become critical gas turbine engine components, which allow turbines to operate at temperatures usually higher or near the melting point of subjacent structural metals. This is in part possible by the TBC's low thermal conductivity [1]. From a general perspective, TBCs are multilayered systems formed by different layers, each complying specific characteristics a) a ceramic topcoat (TC), which provides thermal, mechanical, and physical protection to the system acting as a physical barrier for foreign particles as well as a thermal and chemical insulator; b) a bond coat (BC), which provides adhesion between the TC and the base metal acting as a reservoir of aluminum for the growth of a thermally grown oxide (TGO) and a barrier for oxygen diffusion to the following layer; and c) a nickel-based alloy (SA) as base material which has great phase stability and withstands high mechanical loads. The TC, which is also generically referred to just as TBC, is the outermost layer of the system subjected to direct contact with combustion gases, corrosive conditions of the hottest sections of turbines, and external ingested particles. Among such particles, derivatives from siliceous compounds have been found on in-service failed components and represent a serious threat to the integrity of the TBC [2,3]. Since last decades, the most widely used ceramic material for TBC applications is tetragonal zirconia partially stabilized with 7–8 wt% of yttria (*t'*-7YSZ). The stabilization of the tetragonal phase is given by the presence of yttrium in the lattice [4,5]. Nevertheless, it has been reported that above 1200 °C destabilization of the *t'* phase occurs leading to cubic-monoclinic transformations upon cooling. These phase changes, or phase destabilizations have been associated with coating failure

* Corresponding author.
E-mail address: jmunoz@cinvestav.mx (J. Muñoz-Saldaña).

https://doi.org/10.1016/j.surfcoat.2019.124915
Received 24 June 2019; Received in revised form 15 August 2019; Accepted 18 August 2019
Available online 28 August 2019
0257-8972/

mechanisms, mainly by residual stresses generated by the volume change that accompanies phase transformation [3,6]. The constant increase in operational temperature of turbine engines has reached critical conditions that constraint the 7YSZ phase stability below 1200 °C [7–9]. Above such temperature, other external factors can drastically accelerate the destabilization process.

An example of such factors is the damage of the TBC induced by the ingestion of siliceous airborne dust and debris. When ingested by the turbine, these particles stick, melt, and infiltrate into the porous coating at high temperature, leading to failure [3].

7YSZ-based TBCs are commonly produced either by atmospheric plasma spray (APS), or electron-beam physical vapor deposition (EB-PVD) [10]. The use of one or the other relies on desired characteristics and application of the final coating considering differences in microstructural features achieved by each technique.

Among microstructural features, the porosity of TBCs plays a preponderant role on infiltration kinetics of low viscous or liquid deposits. EB-PVD-produced TBCs consist of columns that grow perpendicularly to the deposition axis. The free space allocated among columns is known as inter-columnar gaps. In general, columnar gaps show similar geometric characteristics and are homogeneously distributed on the coated surface. Inter-columnar gaps represent the overall porosity of the coating and represent the open path through which the melt will flow during infiltration processes. In contrast, APS coatings consist of droplets of material solidified on the top of each other in an unordered manner. The random allocation of solidified droplets results in randomly distributed voids leading to thermal spray characteristic porosity. Given the nature of its formation, porosity is uneven both in size and distribution along the coating. Even though, constructional void porosity may or may not be interconnected. Only interconnected porosity will provide an open path for the flow of melts and thus, infiltration kinetics varies drastically among EB-PVD and APS produced microstructures.

Since the early 90s, interaction of Si-based debris with TBC systems has been an ever-growing concern for the lifetime and performance of high temperature components used in air transportation [11,12]. Obstruction of cooling vane channels and mechanical erosion of in-service helicopter components in desert areas were reported elsewhere and connected to the presence of sand [13]. Sediments found in such in-service airfoils of aircraft engines are mainly composed by Ca, Al, Mg, and Si [13]. Oxides and compounds of such elements have been grouped within the family of the so-called calcium-magnesium aluminum–silicate (CMAS). In-laboratory replication of CMAS, having a chemical composition similar to those found sediments, has allowed the in-depth study of phenomena related to the interaction of TBCs with sand, dust, debris, and other sources of Si-based oxides under controlled conditions. However, in addition to CMAS, other important sources of Si-based materials such as volcanic ashes (VAs) can be found along the flight paths of an aircraft. The concentration and chemical composition of these airborne particles are dependent on meteorological and geographical conditions where they are found. So far, the majority of studies addressing effects of Si-compounds on TBCs are mainly based on CMAS and artificial volcanic ashes (AVAS) with different chemical compositions [3,14]. Studies performed using real VAs are comparatively fewer than those of CMAS, being some of these reported ashes from the Eyjafjallajökull and the Sakurajima [15] volcanos located in Iceland and Japan, respectively. Such studies, addressing infiltration kinetics of VAs have focused mainly on EB-PVD-produced TBCs.

In 2010 the occurrence of the eruption of the Eyjafjallajökull volcano highlighted the threat imposed by natural Si-based sources, such as airborne VAs in the safety and integrity of turbine engines [13,16]. Even when VAs and CMAS share the presence of the main oxide components (Si, Ca, Al and Mg), the latter obviate the presence of other elements. Silica (SiO_2) and calcia (CaO) are reported to be compounds with more influence on TBC degradation [3]. Silica has been directly related to the viscosity of the Si-based melt. Meanwhile, calcia content has been reported to have a great impact on the reactivity of glass. For instance, an increase of 15 to 44% of infiltration depth has been detected by enrichened CaO CMAS. This has been attributed to $CaSO_4$ decomposition and incorporation to the melt, which arguably generates eutectics depending on the overall chemical composition of the glass [17,18]. VAs contain much higher contents of silica and lower contents of calcia than CMAS. Studies with relevance to air transportation of physicochemical properties of ashes from different volcanoes have been reported for several geographic locations around the world [15,18]. Such studies show a wide range of SiO_2 and CaO contents among VAs from 53 to 77 and 2 to 11 mol%, respectively. In the case of CMAS, reported values fluctuate from 23 to 50 mol% of SiO_2 and from 11 to 38 mol% of CaO. Overall SiO_2 contents of CMAS and VAs are reported from 23 to 77 mol% of SiO_2 and from 2 to 38 mol% of CaO [14,17,19–23]. Nevertheless, despite such significant differences in chemical composition, few studies directly address the interaction of VAs with TBCs, and from those only Sakurajima and Eyjafjallajökull have been evaluated [15]. The content of silica in CMAS and VA is responsible for most of its physical properties such as glass transition and viscosity which are relevant for high temperature damage and infiltration on TBCs. Thus, big differences in infiltration behavior between VAs and CMAS in TBCs are expected. Even with this background, there is a lack of reports regarding infiltration phenomena for such natural sources of silica-based melts.

Popocatepetl [24] and Colima [25] are two highly active volcanos located in central Mexico. Due to their volcanic activity, these volcanoes represent a continuous risk for aviation due to their geographic location in one of the most intense air traffic corridors for air transportation in North America but the interaction of these Mexican VAs with TBCs has not yet been reported. The infiltration behavior at 1250 °C of pure volcanic ashes (Popocatepetl 2016, Colima 2015, and Eyjafjallajökull 2010) having a wide range of SiO_2 and CaO content with 7YSZ TBCs produced by APS is addressed in this work.

The main goal of this contribution is to establish the importance of VAs properties for their infiltration behavior and depth, as well as the correlation of such properties with their capability to destabilize 7YSZ TBCs at high temperatures. For this, isothermal infiltration experiments within melting range of VAs on APS-produced TBC were performed. Additionally, mixtures of feedstock 7YSZ powder and as-received volcanic ashes were subjected to heat treatments to determine phase changes as a function of time.

2. Experimental description

2.1. TBC deposition

7YSZ coatings were produced from commercially available powder feedstock (204NS, Oerlikon Metco) by atmospheric plasma spray (APS, Sulzer Metco 9 MB, Wohlen, Switzerland). TBC deposition conditions are given in Table 1 [26]. Before ceramic deposition, a ~58 μm thick NiCoCrAlYTa (Amdry 997, Oerlikon Metco) bond coat layer was deposited by a high velocity oxy-fuel (HVOF) gun [27] (Sulzer Metco

Table 1
Processing parameters for the deposition of 7YSZ coatings by APS.

Current (A)	Voltage (V)	Ar flow (SLPM)	H_2 flow (SLPM)	Stand-off distance (mm)	Powder feed rate (g/min)
565	65	80	15	105	40

DJ2700 Wohlen, Switzerland) operated with propane on an M247-graded single crystalline nickel-based superalloy substrate (Bayreuth Universität, Bayreuth, Germany).

2.2. Characterization of volcanic ashes

Three natural VAs from Colima and Popocatepetl, Mexico and Eyjafjallajökull, Iceland were collected from site during recent volcanic exhalations. Chemical compositions of VAs were determined by optical emission spectroscopy (ICP-OES, Ultima-2, Horiba, Japan). Melting behavior was determined by differential scanning calorimetry with a heating rate of 10 K/min in air, using platinum crucibles (DSC, Setsys Evolution, Setaram, Caluire France). Additionally, crystalline phases of as-received and of isothermally (heat/cooling rate of 10 °C/min) heat-treated VAs between 1 and 10 h at 1250 °C were identified by X-ray diffraction (XRD, Siemens D5000, Karlsruhe, Germany) from 15 to 70° in 2θ, with a 0.5°/min scan rate using CuK_α (1.5406 Å) radiation with a secondary graphite monochromator.

2.3. Infiltration experiments

For infiltration experiments, VAs were deposited on top of TBCs' surface with a concentration of 20 mg/cm^2. To avoid spillage of ashes, before them being properly positioned an adhesive mask with known area was put over the as-coated surface of samples, and then carefully removed before heat treatments. This mask helped also to assure that the whole amount of ashes was set over the required area. Infiltration was performed under isothermal conditions in air using a box furnace at 1250 °C from 1.5 to 10 h with heating/cooling rates of 10 °C/min. Temperature was chosen based on DSC results (Fig. 2) to assure that the three VAs had reached melting range temperature and thus, that they will flow through the porosity of the TBC. Standard metallographic techniques were used to prepare cross-sections to determine the infiltration profile by scanning electron microscopy (DSM ultra 55, Carl Ziess NTS, Wetzlar, Germany). Infiltration depth was confirmed by microstructural analysis and element tracking of cross-sectioned TBCs using energy dispersive x-ray spectroscopy (EDS, Aztec, Oxford Instruments, Abingdon UK). Reaction products at the TBC-VA interface were determined by combining EDS and XRD results.

2.4. Phase identification using XRD studies

Chemical reactivity and corresponding phase formation between 7YSZ powders with respective VAs was studied at high temperatures. For this, feedstock 7YSZ powder and as-received volcanic ashes were mixed and isothermally heat-treated in a box furnace for 2, 5, and 10 h at 1250 °C with a heating/cooling rate of 10 °C/min on platinum sheets. The used 7YSZ / VA proportion was 60 / 40 wt% following similar analyses previously reported in the literature [15]. Heat-treated powders were mechanically removed from the Pt sheets and crushed for XRD analysis. XRD patterns of the as-coated TBC were also taken as reference.

3. Results

3.1. Microstructure of as-coated TBCs

Fig. 1a shows a cross-sectional SEM image of as-prepared APS coatings. Measured thickness of the 7YSZ layer was ~508 μm. As shown in Fig. 1b, a standard APS microstructure with characteristic splat 'brick-wall' morphology is observed. Measured cross-sectional porosity using imaging software (ImageJ) was ~8.5%. As expected for plasma sprayed coatings, roughness value R_a is ~ 8 μm in average (Surftest SV2100, Mitutoyo, Japan). Fig. 1c shows the diffraction pattern of the as-coated TBC. Monoclinic phase content ($\%_m$) of the coatings was calculated to be 1.91% relative to the tetragonal phase as expressed in Eq. (1), considering the intensity of the $\bar{(}\bar{1}11)$ and (111) peaks of the monoclinic, and the (101) tetragonal signal from the XRD pattern [28]. The amount of monoclinic phase in as-coated specimens has been related to processing conditions and feedstock material properties. Control of the porosity of the coatings was favored over phases content control and thus, no further efforts were put into reducing monoclinic content. However, the measured amount of monoclinic phase is in agreement with experimental results reported for similar processing conditions. In addition, monoclinic content is often no longer reported in recent literature [26,29,30].

$$\%_m = 100 * \frac{I_m(\bar{1}11) + I_m(111)}{I_m(\bar{1}11) + I_m(111) + I_t(101)} \quad (1)$$

3.2. Characterization of volcanic ashes

Oxide content analyses of VAs in the literature as well as in this manuscript are based on the measurements of the elemental composition, which is later expressed in terms of their most common or stable oxides (e.g. the elemental quantification of Si is expressed as SiO_2 content). This does not necessarily imply that the source of such sediments contains exclusively those oxides but that they can be present in a wide number of crystalline or amorphous phases within the actual source. The studied VAs presented a wide range of SiO_2 content (57.9, 77.0 and 80.7 mol% for Eyjafjallajökull, Colima, and Popocatepetl, respectively, Table 2). Mexican volcanic ashes present low CaO contents (5.6 and 3.2 mol% for Popocatepetl and Colima, respectively) compared with the Eyjafjallajökull VA (11.5 mol%). Further on, iron content is significantly lower in Mexican VAs compared to the Iceland source. On the contrary, in addition to the higher content of SiO_2, presence of sodium oxide is considerably higher in Mexican sources.

DSC for Eyjafjallajökull (Fig. 2) volcano illustrates glass transition temperature around 750 °C, above that temperature a clear endothermic peak T_{1E} is observed around 775 °C. Two more additional endothermic signals are found at 968 and 1015 °C denoted as T_{2E} and $T_{3E,}$ respectively. The beginning of melting range is observed at around 1035 °C and prolonged up to 1180 °C. Given the complex nature of volcanic ashes it is rather complicated to attribute those signals to specific thermal events. However, such peaks suggest phase transformations within the samples before the melting range begins. Additionally, a series of additional *endo*-exothermic peaks after the melting range temperature suggest further phase transformations at high temperatures in the semi-molten or low viscous state. In the case of Colima VA, glass transition is barely detected between 685 and 890 °C. Also, an exothermic peak around 1060 °C T_{1C}, can be observed. After T_{1C}, a pronounced endotherm indicates the beginning melting range (around 1060 °C). Further endothermic signals seen above 1160 °C seem to be related to melting or phase transformation of minor phases present in the VA. Analogously, glass transition of Popocatepetl VA is also slightly observed between 727 and 904 °C. Afterwards, one exothermic peak suggesting intermediate crystallization processes can be seen at 1185 °C, T_{1P}. The end of T_{1P} leads to the start of the melting range at 1185 °C. Above 1265 °C, a number of endo – exothermic peaks related to further phase transformation and melting of remnant phases are detected. In general, as pointed out in Fig. 2, at 1250 °C tested VAs lie within the melting range. At such temperature, calculated viscosities are of 2.92, 4.06 and 4.35 log (Pa*s) for Eyjafjallajökull, Colima, and Popocatepetl, respectively. These values were calculated according to Giordano's model for viscosity of melts based on chemical composition [31]. DSC analyses presented in Fig. 2 were carried out principally to determine the melting range of the ashes to perform infiltration experiments. Phase transformations given by the rest of *endo*-exothermic signals are not in the scope of this work and will not be further discussed.

X-ray diffraction patterns in Fig. 3a show that Eyjafjallajökull ashes are mainly constituted by amorphous phases in the as-received state.

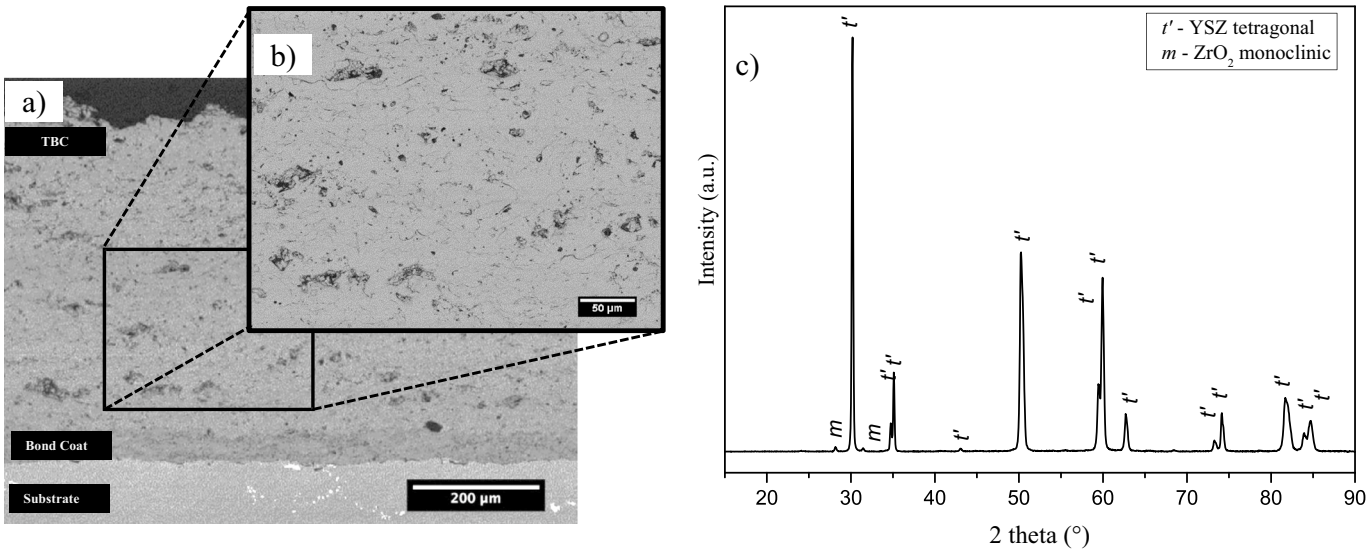

Fig. 1. Characteristics of the as-coated samples used in this work showing a) a general view of the TBC b) a high magnification micrograph of the microstructural characteristics of the as-coated 7YSZ layer and c) the XRD pattern indicating the main peaks for tetragonal (*t*) and monoclinic (*m*) phases.

Table 2
Chemical composition of volcanic ashes.

Source	Chemical composition (mol%)							
	SiO_2	TiO_2	Al_2O_3	FeO_T	MgO	CaO	Na_2O	K_2O
Popocatepetl	80.7	1.3	2.1	3.6	0.1	3.2	8.0	0.18
Colima	77.0	0.8	4.3	4.1	0.3	5.6	7.9	0.16
Eyjafjallajökull	57.9	5.3	5.6	12.3	3.1	11.5	4.5	0.15

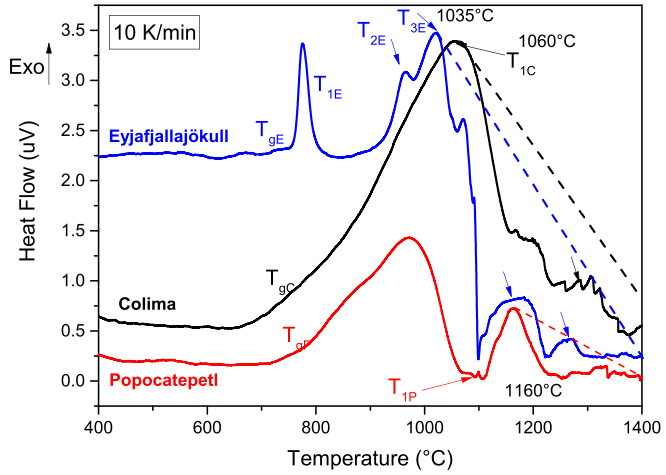

Fig. 2. DSC curves for a 10 K/min heating rate of the as-received volcanic ashes in the range of 400 to 1400 °C. Within the curves glass transition (T_{gx}) and endothermic peaks (T_{nx}) temperatures are indicated. x denotes E for Eyjafjallajökull, C for Colima and P for Popocatepetl. The melting range is also indicated by dashed lines of each curve.

This particular VA contains the least amount of SiO_2 and the highest content of FeO_T and TiO_2 among tested ashes (Table 2). Crystallinity of such ashes increases with the heat-treatment time between 2 and 10 h. In the as-received state the main phases include anorthite $CaAl_2(SiO_4)_2$, α, wollastonite $Na_2Ca_3Si_6O_{16}$, ω and diopside ($CaMgSi_2O_6$) δ. Weak signals corresponding to hematite Fe_2O_3, ε, iron-titanium oxide $Fe_{1.696}Ti_{0.228}O_3$, η, and calcium-sodium-aluminum oxide $Ca_{8.25}Na_{1.5}(Al_6O_{18})$, φ, are also detected. After thermal treatments, two main effects are seen. First, for intermediate times (1–5 h) the amorphous phase content decreased arguably due to the low network-formation capabilities of the glass related to Ti^{4+}, Al^{3+}, and Fe^{3+} contents [32]. Second, diopside, wollastonite, and calcium-sodium-aluminum oxide are no longer found as crystalline phases in the heat-treated sample. On the other hand, the signal corresponding to anorthite does not present a significant change. Moreover, signals related to hematite and iron-titanium oxide show an evident increase in intensity. Finally, after 10 h, XRD patterns show the presence of almost exclusively hematite overlapping with iron-titanium oxide and srebrodolskite, $CaFeO_4$, *σ*. Contrary to what was observed in Iceland ashes, as-received Mexican VAs are crystalline in nature presenting peaks that match with albite $(Na,Ca)Al(Si,Al)_3O_8$, γ, andradite $CaFe_2SiO_4Ti$, β, anorthite/anorthite sodian $CaAl_2(SiO_4)_2$ /$(NaCa)(AlSi)_4O_8$, α, and pyroxene $Mg_2SiO_2O_6$, π. Main peaks correspond to anorthite/anorthite sodian. Signals between 27 and 32° in 2 theta can also overlap to the main peaks of diopside ($CaMgSi_2O_6$) and other members of the plagioclase family $(Na,Ca)(Si,Al)_3O_8$ such as oligoclase and labradorite. Both Colima and Popocatepetl ashes exhibit clear transformation after 10 h heat treatments from the initial crystalline state into amorphous glass (Fig. 3b and c) arguably due to the high content of SiO_2. At this temperature, both VAs patterns suggest that albite, and andradite are the first phases to turn into an amorphous state followed by pyroxene. Anorthite/anorthite sodian seem to be the last phases to transform into glass. Measured XRD patterns in the as-received VAs are in agreement with literature results that include the presence of plagioclases from albite and anorthite for both natural and artificial ashes [14,15,33]. However, a detailed description of changes in phases and crystallinity as a function of time is not available for comparison.

3.3. Infiltration experiments

7YSZ APS coatings were subjected to isothermal heat-treatments at 1250 °C to promote VAs infiltration. Due to high temperature, the Ni-based substrates suffered severe oxidation. As a result, all the coatings have been peeled off from the substrate during the thermal treatments. However, infiltrated 7YSZ coatings were used in the free-standing coatings condition *as infiltrated* as no damage to the coating was observed, thus allowing to proceed with the infiltration analyses via SEM.

The microstructural differences between the as-coated (non-infiltrated) TBCs and the regions infiltrated with Eyjafjallajökull, Colima and Popocatepetl ashes are shown in Fig. 4a-d, respectively. In the infiltrated samples (Fig. 4b-d), inter-splat gaps are no longer well defined

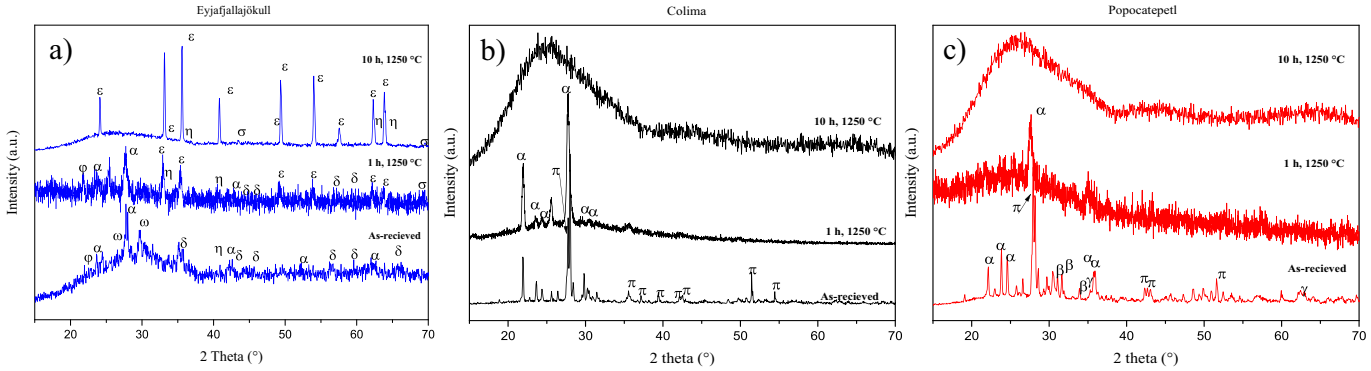

Fig. 3. X-ray diffraction patterns of ashes from a) Eyjafjallajökull, b) Colima and c) Popocatepetl volcanoes showing, from bottom up, as- received, 1 h, and 10 h of isothermal heat treatment at 1250 °C.

when compared with the non-infiltrated microstructure (4a). These microstructural differences are related to specific phase transformations. For instance, through EDS and XRD analyses the globular-shaped microstructure seen in the samples have been associated in the literature with the tetragonal to monoclinic zirconia phase transformation around the CMAS infiltrated zones [14,34–36]. This has also been reported by TEM structural analyses [17,37–39]. The formation of monoclinic zirconia brings concomitant chemical composition changes both in the ceramic TBC and in the surrounding glass, which has been confirmed in the analysis of reaction products.

A general view of the cross-section microstructural features of the samples infiltrated for 10 h allows for a depiction of an infiltration profile (Fig. 5a-c). These infiltration profiles are in agreement with Si contents measured with point EDS analyses. Infiltration depth of the VAs on all samples was measured by identifying Si contents and the correspondent microstructural changes by image analysis (ImageJ). Infiltration depths are plotted as a function of time (Fig. 6), showing that the infiltration depth increases as SiO_2 content decreases. After 10 h of heat treatment the maximum measured infiltration depths were 440 μm for Eyjafjallajökull, 269 μm for Colima and 247 μm for Popocatepetl. Infiltration speed or infiltration rate of the VAs, given by the slope of the plots shows a non-linear behavior. From this, two different regimes are identified. A faster infiltration rate regime is observed during the first 2 h with values of 2.50, 1.41, and 1.24 μm/min for Eyjafjallajökull, Colima, and Popocatepetl, respectively. After 120 min, infiltration rates abruptly decrease to a low infiltration rate regime of 0.286, 0.212, and 0.214 μm/min for Eyjafjallajökull, Colima and Popocatepetl. Infiltration curves show a drop in the infiltration rate between 1/8th and 1/5th of the initial values (first120 min). As seen, this abrupt change in infiltration rate is consistent among the three VAs tested. Such behavior predicts that the initial first 2 h of exposure to high temperatures is critical on the infiltration depth.

3.4. High temperature powder reactions

Reaction products near the VA-7YSZ interface of the long-term heat-treated samples (10 h) were identified by matching their chemical composition from the EDS measurements with stoichiometric values of

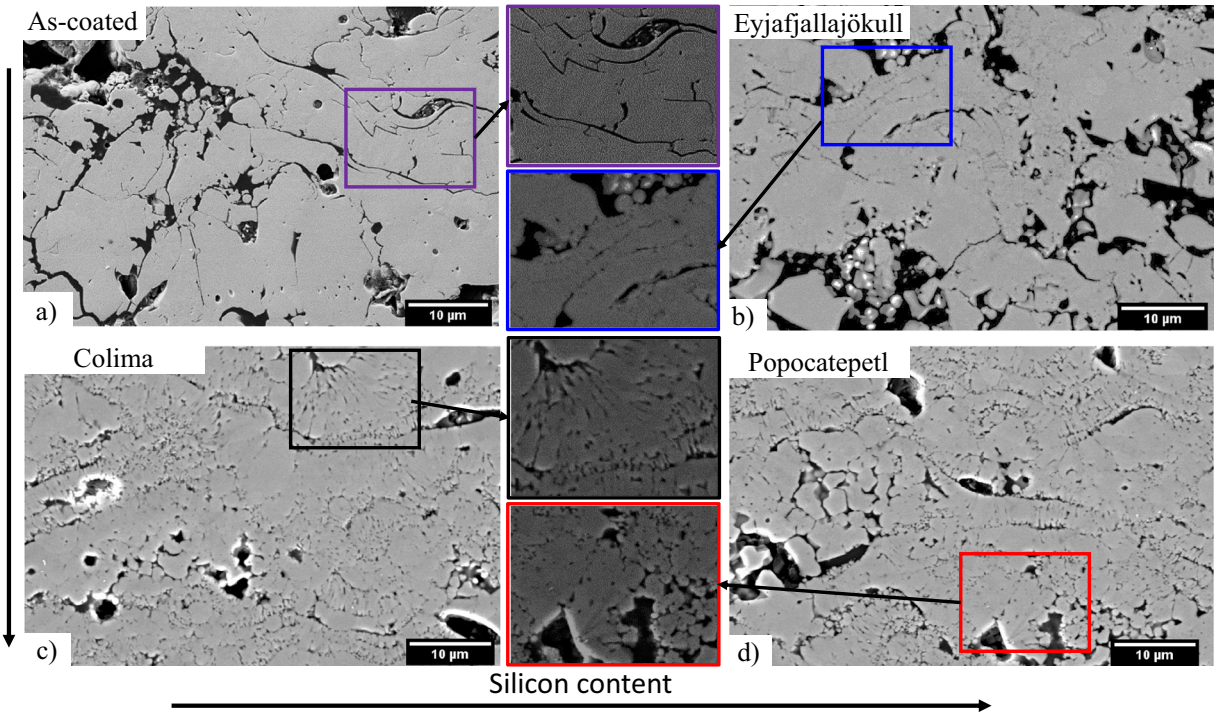

Fig. 4. High magnification SEM micrographs showing microstructural differences between the a) as-coated and 10 h heat treated coatings b) Eyjafjallajökull c) Colima, and d) Popocatepetl. Changes include the formation of globular shaped crystals which are more evident as SiO_2 content in VA increases form b) to d).

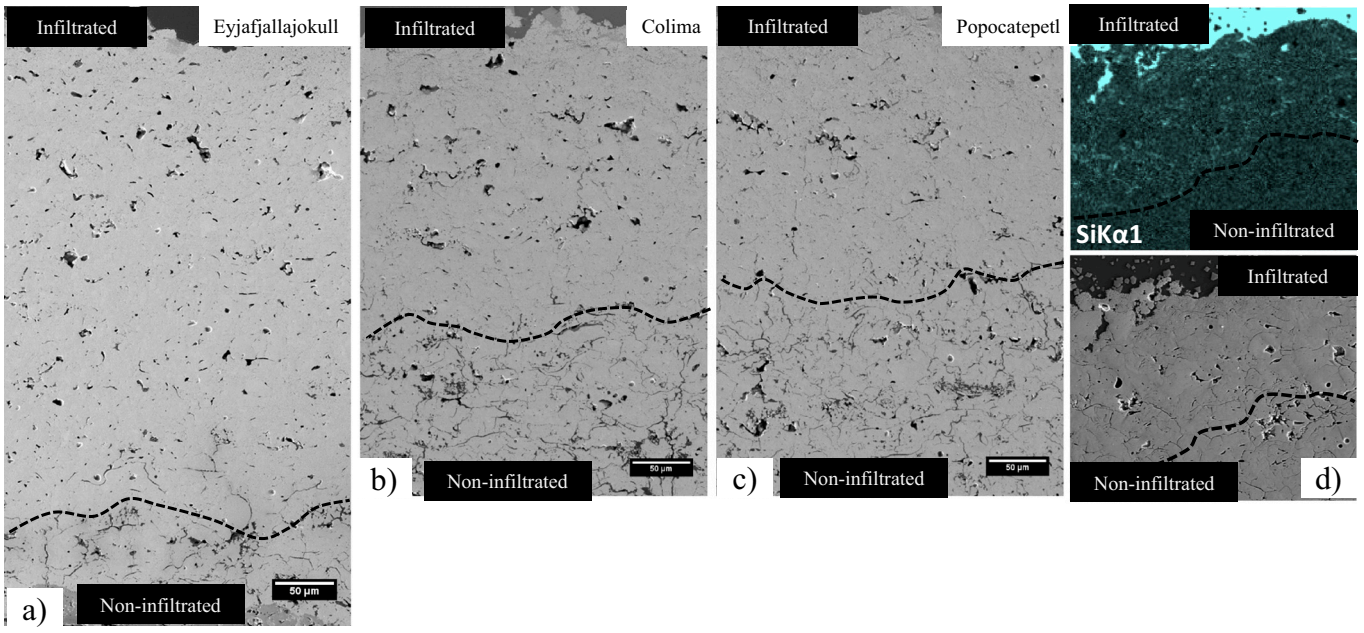

Fig. 5. SEM micrographs showing the general view of the samples after 10 h heat treatments. A depiction of the limit of infiltration is indicated (dashed line) for a) Eyjafjallajökull, b) Colima, and c) Popocatepetl. Figure d) shows a general representation of Si mappings used to confirm infiltration depths of the samples.

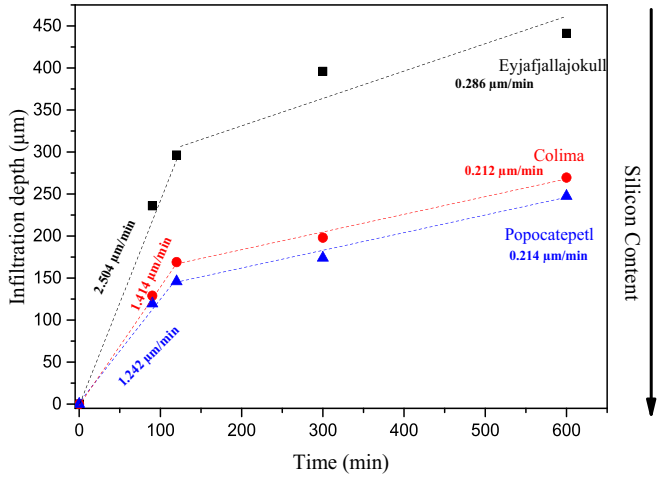

Fig. 6. Curves of the measured infiltration depth as a function of time for the different VAs. Figure shows abrupt changes of the infiltration rates around 120 min. Values of these infiltration rates before and after this time are shown for each VA.

particular phases and compared with the XRDs of respective powder mixtures. Fig. 7a-c show the general overview of the VA-7YSZ reacted interface for Eyjafjallajökull, Colima and Popocatepetl, respectively. Fig. 7d-f are micrographs recorded at higher magnifications where the reaction products have been identified. Globular crystals, denoted as *m*, matching the chemical composition of *m*-ZrO_2 are observed near the glass/coating interface. In addition, zones denoted as $t' + m$ indicate the presence of yttrium and zirconium in a non-stoichiometric ratio and are therefore considered as a mixture of 7YSZ and *m*-ZrO_2. Measurements of the glass deposit near the interface show traces of zirconium and yttrium, which indicates their depletion from the TBC into the melt, and the possible interaction of Si with Zr leading to the formation of $ZrSiO_4$. EDS spot analyses revealed that partially destabilized crystals ($t' + m$) also include de presence of Fe and in some cases Ca and Al. However, elements as K, Na or Mg, have not been detected in the identified reaction products for any of the VAs. Table 3 shows the EDS spot analyses results for the different samples as well as expected values for stoichiometric phases.

In addition to microstructural EDS analyses, powder mixtures containing 60 wt% of feedstock 7YSZ and 40 wt% of volcanic ashes were heat treated at 1250 °C from 2 to 10 h. The XRD patterns of the as-coated samples were also measured as a reference. X-ray diffractograms recorded after different heat-treatment time are presented in Fig. 8. From these results the following observations can be raised.

a) Eyjafjallajökull VA-7YSZ interactions (Fig. 8a): The signal related to the monoclinic peak reaches a maximum at 2 h. Meanwhile, the zircon-related peak is more intense in the 5 h sample. After 10 h, both monoclinic and zircon-related signals have significantly decreased.

b) Colima VA-7YSZ interactions (Fig. 8b): A maximum for zircon is observed after 2 h, whereas the monoclinic peaks show greater intensity in the 5 h sample.

c) Popocatepetl VA-7YSZ interactions (Fig. 8c): A maximum of the monoclinic and zircon signals is observed after 2 h to then continuously drop until 10 h.

Three VAs show that after 10 h of heat treatment both zircon and monoclinic have decreased respect to the detected maximum in shorter time. The content of monoclinic phase was estimated with Eq. (1) [28]. Monoclinic content curves sum up the tetragonal to monoclinic transformation behavior as a function of time (Fig. 9a). As mentioned before, there is a maximum around 2 h for Eyjafjallajökull and Popocatepetl and 5 h for Colima. Regarding the zircon content, even though the quantification was not possible, change in relative intensity of $ZrSiO_4$ signal follows a trend described before and is shown in Fig. 9b. From the obtained results it can be inferred that the formation of main reaction products (*m*-ZrO_2 and $ZrSiO_4$) is not linearly dependent on time.

4. Discussion

The high influence of the chemical composition of the VAs on the infiltration kinetics was confirmed. However, contrary to what was expected, infiltration rates show different values as a function of time in all cases. Second, destabilization capabilities of the VAs also depend on the chemical composition. As mentioned before, this is defined by the variation of relative content of monoclinic zirconia and zircon as a function of time. The destabilization behavior varied as a function of time. These observations seem to be directly correlated with the

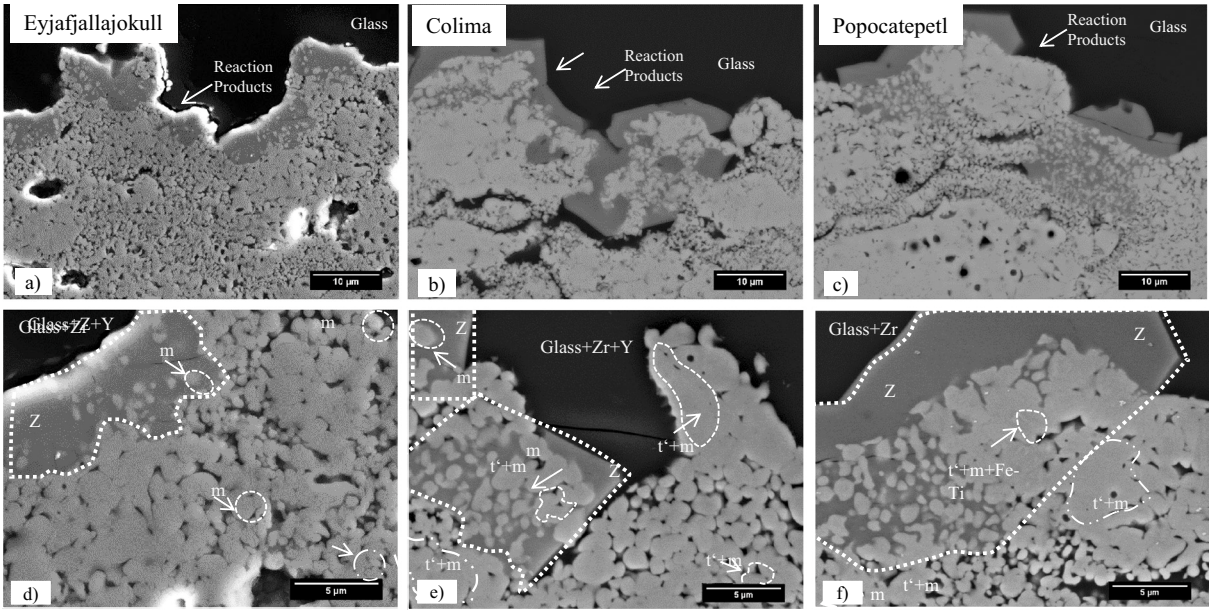

Fig. 7. Representative SEM micrographs of infiltrated TBCs. On top, general overview of the glass/7YSZ interface for Eyjafjallajökull, Colima, and Popocatepetl. On the bottom, high magnification images of the interfaces showing the different reaction products obtained after 10 h of heat treatment. In them, the presence of $ZrSiO_4$ is denoted as *Z*, monoclinic ZrO_2 as *m*, tetragonal 7YSZ as *t*. *t* + *m* denotes a non-stoichiometric Y—Zr ratio, which is assumed to be a monoclinic + tetragonal mixture. *Glass* + *Z* and *Glass* + *Y* denotes de dissolution of Zr and Y into the glass.

Table 3
Atomic chemical composition of EDS spot analyses for VA-7YSZ TBCs interactions for 10h at 1250 °C. Also, stoichiometric content for *m*-ZrO_2, *t*'-7YSZ and $ZrSiO_4$ are shown.

(at.%)

Label	Zr	Y	Si	Fe	K	Ca	Ti	Na	Mg	Al	Corresponding phase
Stoichiometric phases											
m	100										*m*-ZrO_2
t'	96.5			1.6			1.8				7YSZ
Z	50		50								$ZrSiO_4$
Eyjafjallajökull-7YSZ											
m	100										*m*-ZrO_2
m + Fe + Ti	96.5			1.6			1.8				$Zr_{0.29}Ti_{0.006}Fe_{0.004}O_{0.70}$
Z	54.4		45.5								$ZrSiO_4$
Glass +Zr	57.9		42.0								Glass + Zr
Colima-7YSZ											
t' + m	90.4	9.5									$Zr_{0.34}Y_{0.03}O_{0.62}$
t' + m + Fe	92.7	5.1		2.1							$Zr_{0.35}Y_{0.019}Fe_{0.008}O_{0.62}$
m	100										m-ZrO_2
Z	50.2		49.7								$ZrSiO_4$
Glass +Zr + Y	1.5	1.9	56.5	3.2	1.0	6.6	0.4	5.1	2.9	20.7	Glass + Zr + Y
Popocatepetl-7YSZ											
t'+m-Fe-Ti	93.9	3.6		1.4			0.9				$Zr_{0.35}Y_{0.01}Fe_{0.005}Ti_{0.36}O_{0.62}$
t'+m	94.7	5.3									$Zr_{0.34}Y_{0.019}O_{0.63}$
m	100										m-ZrO_2
Z	51.4		48.5								$ZrSiO_4$
Glass+Zr	1.9		59.5	4.2	1.5	6.0	0.6	4.4	3.2	18.5	Glass + Zr

chemical nature of volcanic ashes and will be discussed deeper in the following sections.

4.1. General nature and melting behavior of VAs

ICP chemical analyses showed that the main chemical differences among VAs are SiO_2, CaO, TiO_2, FeO_T, and Na_2O contents (Fig. 2). Attempts to use specific basic/acidic oxides ratios as numerical parameters for infiltration and reactivity degree have been reported elsewhere [40,41]. It is generally accepted that the variation of acidic oxides (e.g. SiO_2) and basic oxides (e.g. CaO) has major influence on the infiltration behavior and reactivity of VAs-CMAS/TBCs interactions. SiO_2 has been addressed as the most relevant element regarding infiltration properties specifically affecting the viscosity. The effect of chemical composition on the viscosity as a function of temperature has been approached in the literature with a mathematical model based on stable oxides content [31]. By using such model, it can be seen in Fig. 10 how the SiO_2 content drastically affects viscosity values. A comparison between VAs and CMAS viscosity calculated using the Giordano model is given as a reference to illustrate that VAs have a viscosity of orders of magnitude higher than that reported for CMAS. Even when discrepancies between calculated values and experimental

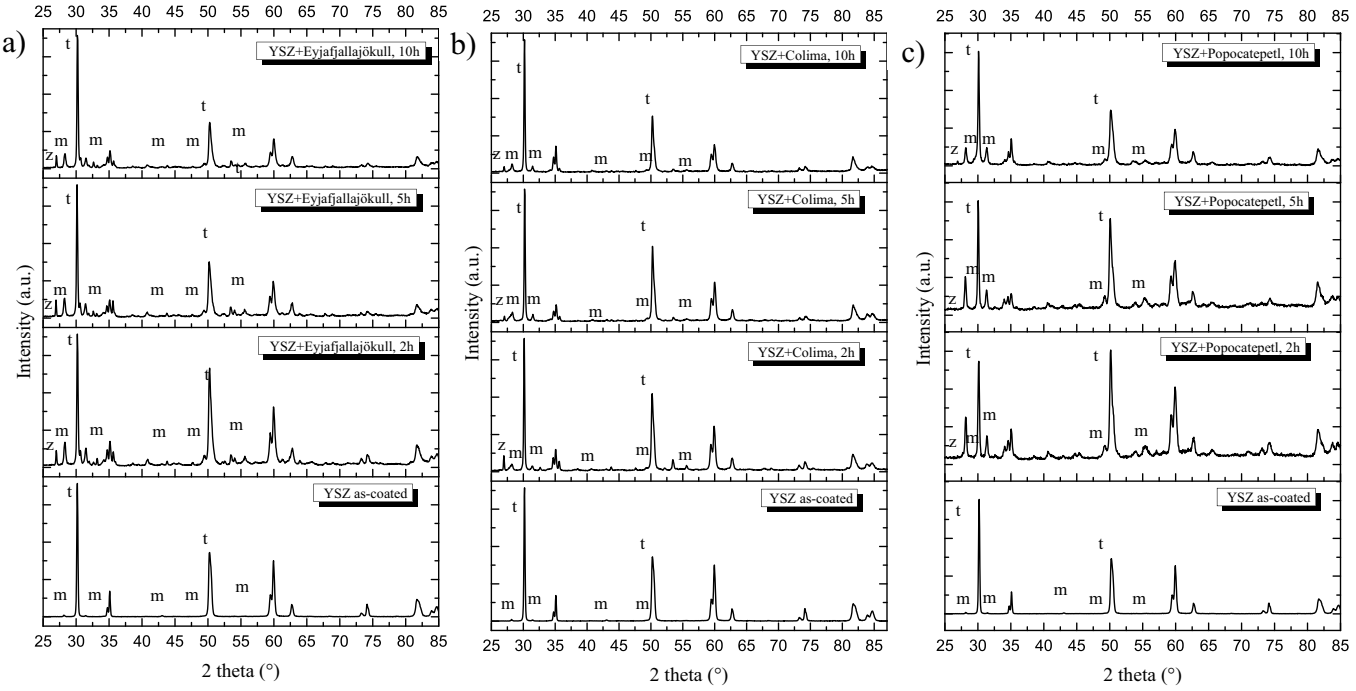

Fig. 8. X-ray diffraction patterns for the powder mixtures (60%wt 7YSZ, 40% VA) of a) Eyjafjallajökull, b) Colima and c) Popocatepetl showing from bottom up, 2 h, 5 h and 10 h of heat treatment at 1250 °C. Peaks corresponding to main phases are identified as *m* for monoclinic ZrO_2, *t* for tetragonal 7YSZ and *Z* for zircon.

results have been reported and discussed [42], the trend indicates that the infiltration depth of VAs is expected considerably lower than that of CMAS. This assumption is in accordance with both literature and experimental results presented here.

Again, different chemical composition of VAs defines its melting behavior, constituent oxides transformation, and possible cationic substitutions upon cooling from the molten state [33,43]. However, additional differences in melting behavior can be related to particle size distribution and humidity content of VAs. All these characteristics are indeed difficult to replicate in the laboratory and thus, a real approach using natural sources for Si-based materials such as VAs is pertinent for understanding infiltration and chemical reactions with TBCs interactions [15,19,33,43].

DSC analyses (Fig. 2) show the complexity of the thermal behavior of the tested VAs samples. The observation with main relevance for this work is the identification of the melting range temperature for each VA which increases as the SiO_2 content increases. This may be expected when observing the CaO-SiO_2 phase diagram, where it can be seen that as composition moves further away from the eutectic point (around 63 wt%), melting temperatures will increase until around 95 wt% [44]. The occurrence of endothermic peaks below melting range temperature has been previously reported and been associated with phase transformations [45]. Structural differences among VAs after heat treatments can then be associated with the high iron content and relatively low content of SiO_2 of Eyjafjallajökull, compared to the very high SiO_2 and low FeO_T content of Colima and Popocatepetl. Endo-exothermic peaks after melting ranges can be associated with high temperature phase transformations. In the case of Colima and Popocatepetl they can be related to the formation of amorphous phases and the decomposition of andradite to pseudowallastonite and hematite. On the other hand, for Eyjafjallajökull, containing high FeO_T and low SiO_2, the transformation seems to occur in the opposite way. In such case the predominantly amorphous phase with low contents of anorthite, diopside, hematite and iron-titanium oxide turn to predominately crystalline hematite and iron-titanium oxide.

For Si-rich VAs albite is the first phase to turn into an amorphous

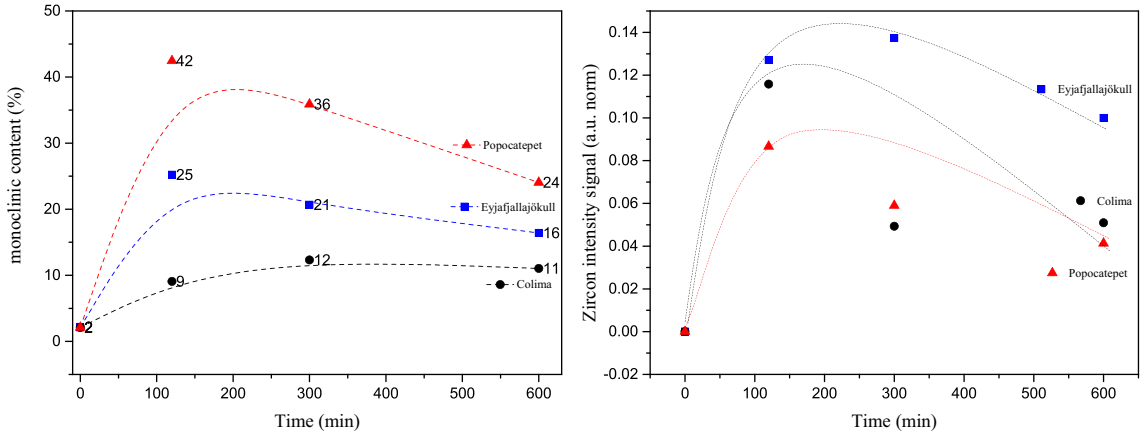

Fig. 9. a) Curves of the calculation of the *m*-ZrO_2 content in the powder mixtures (60%wt 7YSZ, 40% VA) according to Eq. (1) [28] for the three tested VAs. b) plot of relative intensity changes of zircon peaks as a function of heat treatment time for each VA.

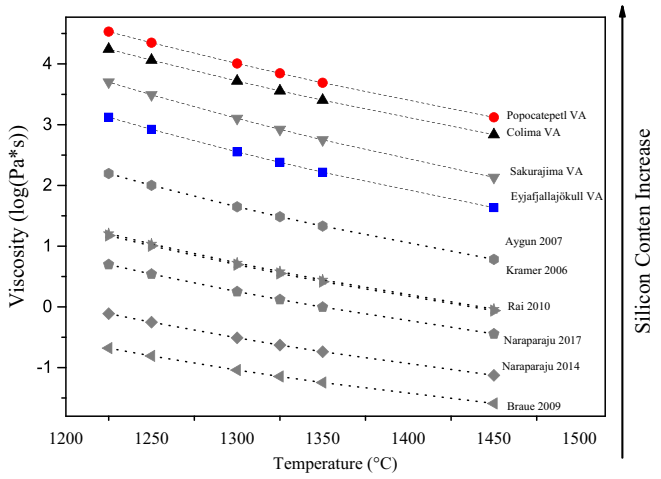

Fig. 10. Viscosity curves of tested VAs calculated from chemical composition values using the Giordano et al. model [31]. Reported viscosities of CMAS and other VAS are also shown in gray as reference [15, 17, 18, 20–22].

phase. Meanwhile, andradite undergoes decomposition behavior to pseudowallastonite and hematite both having a melting point around 1540 °C [46]. Last phase to turn into glass is anorthite/anorthite sodian having a melting point of 1555 °C as a pure substance. Melting range temperatures of the VAs are below the melting point of pure substances due to the interaction of all the different chemical species on the sample which changes the kinetics of internal phase transformations. However, the melting sequence is as expected based on melting temperatures reported for main individual phases [47]. Reported CMAS contain far smaller amounts of SiO_2 compared to VAs, exhibiting crystalline nature as long as they contain FeO_T.

Structural changes detected through XRD for the heat-treated VAs are mainly related to crystalline to amorphous and amorphous to crystalline phase transformations as heat treatment time increased. The conditioning factor for the occurrence of one or the other of the above-mentioned transformations seems to be the iron and titanium content in the as-received ashes. Fe-Ti-rich VAs are amorphous in nature, which is in agreement to work reported elsewhere [33]. On the other hand, it was also reported that ashes containing less Fe—Ti are crystalline in the as-received state to then transform into amorphous with heat-treatment.

4.2. VAs-7YSZ interaction and corresponding phase stability

Phase stability of 7YSZ was studied through analyses of reaction products of heat treated samples in the form of mixtures of feedstock powder and as received VAs. After 10 h of heat treatment, results showed that reaction products are the same for all 7YSZ-VA interactions.

Near the VA/7YSZ interface, *m*-ZrO_2 was found to be embedded in the zircon matrix (Fig. 7). From the microstructure, the growth of zircon crystals seems to advance at the expense of the *m*-ZrO_2 content. This can be specially seen in Fig. 7f where the larger amounts of globular crystals seem to be consumed by the zircon crystal formation leading to an indirect proof that $ZrSiO_4$ forms at the expense of *m*-ZrO_2 once the destabilization of 7YSZ reaches a limit.

On the other hand, from XRD patterns, it is clear that zircon formation also reaches a maximum value below 5 h of heat treatment. Even though feedstock powder -VA ratio for powder mixtures used for the above mentioned experiments differs from the TBC-VA ratio of the infiltrated samples, the results imply a similar behavior.

XRD patterns confirm the presence of *t'*-7YSZ, *m*-ZrO_2, and $ZrSiO_4$ as final products for 10 h heat treatments in accordance to what can be observed in the microstructural analyses. Also, the evolution of *m*-ZrO_2 formation can be seen by the increase of the corresponding peaks until a maximum value is achieved at 5 h for Colima and 2 h for Eyjafjallajökull and Popocatepetl where higher content of SiO_2 enables the formation of higher amounts of *m*-ZrO_2. On the other hand, the intensities of zircon peaks relative to those of *m*-ZrO_2, are stronger for VAs containing low SiO_2 (Eyjafjallajökull). These results are somehow contradictory to what was observed from the microstructural analysis where as silica content increases, the formation of globular crystals seems to increase as well (Fig. 4), and to the prior assumption that higher contents of SiO_2 on the VAs, will result in higher formation of $ZrSiO_4$. However, the physical phenomena involved in this process are not yet understood.

The phase transformation behavior can be classified into three general sections. The first is related to destabilization of the tetragonal 7YSZ transforming into *m*-ZrO_2. This is observed by the great increase of the monoclinic related signal for all samples in the XRD. The second stage includes the formation of zircon ($ZrSiO_4$) through the interaction of the Si-based melt with the *m*-ZrO_2. In such case, zircon signals can also be seen as early as 2 h of heat treatment. Once a maximum *m*-ZrO_2 is reached, the third stage is related to the progress of the continuous destabilization of 7YSZ (at much lower rates), competing with the formation of $ZrSiO_4$ from the Zr—Si interaction and the continuous incorporation of Zr and Y to the melt.

4.3. Infiltration kinetics and microstructural influence

Microstructural changes were identified for the VA-7YSZ isothermal infiltration experiments. Main changes include the modification of the characteristic APS inter-splat boundaries and the presence of tiny globular grains within them, matching chemical composition for monoclinic zirconia. Such small grains seem to coalesce to form bigger *m*-ZrO_2 globes as time increases (Fig. 4b-d).

Concerning TBCs' infiltration, as expected, it was observed that infiltration depth increased as SiO_2 and viscosity decreased. However, infiltration kinetics show a non-expected behavior consistent for the three ashes. According to the measured infiltration depths (Fig. 6), two different regimes with remarkably different infiltration rates were observed opposed to a constant infiltration rate. In the first segment, a high infiltration rate is observed from 0 to 2 h. At this stage, the infiltration rate of Eyjafjallajökull (2.50 μm/min) is higher than Colima (1.41 μm/min) and Popocatepetl (1.24 μm/min). The second segment (from 2 to 10 h) is a low-rate segment, where infiltration rate drops to a virtually same rate for the three ashes being 0.28 μm/min for Eyjafjallajökull and 0.21 μm/min for both Colima and Popocatepetl. When comparing infiltration rates (Fig. 6) with the calculated monoclinic content for different time (Fig. 9a), the high-rate infiltration ($0-2\ h$) seems to be in accordance with the destabilization process of *t*-7YSZ. As mentioned before, the monoclinic phase reaches a maximum content below 5 h of heat treatment for Colima, and below 2 h for Popocatepetl and Eyjafjallajökull. At these maximum points, the monoclinic content has increased from the as-coated content of 2% to 25, 12 and 42% for Eyjafjallajökull, Colima and Popocatepetl, respectively. As infiltration time progresses up to 10 h, monoclinic phase content decreases to 16, 11 and 24%, respectively. This suggests that the chemical reaction between VAs and 7YSZ leads first to formation of the *m*-ZrO_2. The driving force for the destabilization is the local amount of available silicon from the melt. Therefore, VAs with high SiO_2 contents (e.g. Popocatepetl) will destabilize the 7YSZ in greater amount until an equilibrium is reached. This equilibrium is related to the maximum content of monoclinic zirconia (Fig. 9a) and correlated to the high infiltration regime. After equilibrium, the formation of the monoclinic phase is followed by the formation of zircon ($ZrSiO_4$) (Fig. 9b), which is set off by the partial and gradual dissolution of Zr into the glass at expense of the previously formed *m*-ZrO_2 in the adjacent zones of the globular shaped crystals.

Due to this compromise between *m*-ZrO_2 and $ZrSiO_4$, solubility

conditions for Y and Zr in the melts are continuously changing. These competing conditions are alike among different VAs after the formation of zircon begins and thus, infiltration kinetics are considerably similar for different VAs in the low infiltration regime.

Regarding the effect of chemical composition of VAs, TBCs in contact with ashes containing the highest amount of SiO_2 and low contents of Ca and Fe showed the highest monoclinic content for all tested times (Fig. 4 and Fig. 9a). This implies that the destabilization potential of the VA might be more related to the SiO_2 content than to the CaO content.

On the other hand, the presence of zircon (Fig. 9c) seems to be higher in the low SiO_2-containing VA. This suggests that processes of destabilization of t-7YSZ and zircon formation are driven by different factors. As seen in structural changes, Fe-rich ashes turn into crystalline with heat treatment. In additional experiments (not shown here), the presence of Fe—Ti crystals embedded in a glass matrix is clear in heat-treated VAs with high contents of Fe—Ti, whereas the Si-rich VAs do not show any of such crystals. EDS spot analyses near the VA-7YSZ interface after long periods of high temperature exposure to VAs (Table 3) confirm the presence of Fe and Ti within the ceramic coating. From this, it could be inferred that some elements, such as Fe and Ti may act as catalysts for nucleation points in in the formation of zircon, and therefore Fe-Ti-rich ashes promote its formation in higher degree than Fe-poor ashes.

After 2 h of annealing, infiltration rates are seen to be nearly identical for VAs with different chemical compositions. This would indicate the probability of them having similar viscosity values after the above-discussed chemistry changes. An explanation for this can be given if as mentioned, local equilibrium conditions within in the infiltrated gaps are similar for all the VAs after the maximum destabilization of the TBC has been reached. For this, the well-known fact that the 7YSZ-VA interaction does not generate a reaction layer or physical barrier that stops the flow of the melt should necessarily be considered. Instead, the newly Zr-Y-rich melts with lower viscosity will still penetrate the coating, yet at much lower rates.

Through a closer look to the development of the microstructural transformations along the infiltration path, it is clear that the maximum depth at which it occurs is not parallel to the coatings' surface rather than is shows an irregular profile. Such profile can be related to the porosity and other microstructural coatings' features. This points to the importance of porosity, cracks gaps, etc. during high temperature interaction of VAs-7YSZ. This is a clear evidence that in addition to VAs and coatings' chemical nature, microstructural features of TBCs are determinant factors on infiltration behavior. Therefore, further experiments with different degrees of porosity of the TBC are planned to better understand and describe the infiltration kinetics of VAs in TBCs to be able to predict infiltration kinetics for any given Si-based melts.

5. Conclusions

Conducted infiltration experiments and the corresponding phase formation analysis supported by powder mixture investigations of three volcanic ashes led to a number of conclusions regarding infiltration kinetics and reaction products of high-temperature VAs-7YSZ interactions.

5.1 VAs containing high SiO_2 have shown lower infiltration kinetics than those with lower content. This is in accordance to estimations of the relationship between SiO_2 and the viscosity at a given temperature reported in the literature.

5.2 Infiltration of volcanic ashes on 7YSZ TBCs produced by APS show a behavior that is non-linear with respect to time. Instead, variable infiltration rates are observed, which are here classified in high (from 0 to 2 h), and low (from 2 to 10 h) infiltration rates. High infiltration rate has been calculated to be 5 to 8 times greater than the low rate regime.

5.3 In the high infiltration rate regime, a clear dependence between rate and chemical composition of the VA gets obvious: the lower the silicon content and hence the viscosity, the higher is the infiltration rate. However, infiltration rates slow down and show comparable values among different VAs after annealing for more than 2 h due to similar local chemistry in the infiltration process after phase destabilization has reached a maximum.

5.4 Low-infiltration rate is achieved after 2 h, where the Zr—Y incorporation into the glass reaches its limit and changes the local glass composition with modified viscosity.

5.5 In the low infiltration regime, there is a competition between dissolution of Zr—Y into the glass and the reaction of *m*-ZrO_2 with melt to form $ZrSiO_4$.

5.6 The phase destabilization potential of the volcanic ashes is related to their SiO_2 content, higher silica content in the VA seems to enable higher amounts of *m*-ZrO_2 formation. On the other hand, $ZrSiO_4$ formation behaves differently, the lower the content of SiO_2, the higher amounts of zircon formation.

Acknowledgements

Authors thank the Mexican Council for Science and Technology, CONACYT for funding related to this project (293429). Also, thanks to Dr. L. Capra from the Geosciences department of UNAM for providing the Colima and Popocatepetl ashes and to Dr. A. G. Mora-García and Prof. U. Glatzel for providing the SA substrates. J. Muñoz-Saldaña thanks to CONACYT and the Alexander von Humboldt Foundation for financial support for research activities at the German Aerospace Center, DLR. This work has been carried out jointly at CENAPROT and LIDTRA national laboratories in Mexico and the High-Temperature and Functional Coatings department of DLR in Germany.

References

[1] D.R. Clarke, M. Oechsner, N.P. Padture, Thermal-barrier coatings for more efficient gas-turbine engines, MRS Bull. 37 (2012) 891–898, https://doi.org/10.1557/mrs.2012.232.
[2] L. Li, N. Hitchman, J. Knapp, Failure of thermal barrier coatings subjected to CMAS attack, Proc. Int. Therm. Spray Conf. 19 (2009) 77–82, https://doi.org/10.1361/cp2009itsc0077.
[3] C.G. Levi, J.W. Hutchinson, M.H. Vidal-Sétif, C.A. Johnson, Environmental degradation of thermal-barrier coatings by molten deposits, MRS Bull. 37 (2012) 932–941, https://doi.org/10.1557/mrs.2012.230.
[4] H.G. Scott, Phase relationships in the zirconia-yttria system, J. Mater. Sci. 10 (1975) 1527–1535, https://doi.org/10.1007/BF01031853.
[5] P. Duwez, F.H. Brown, F. Odell, The Zirconia-Yttria System, J. Electrochem. Soc 98–99 (1951) 356–362, https://doi.org/10.1149/1.2778219.
[6] D.E. Mack, T. Wobst, M.O.D. Jarligo, D. Sebold, R. Vaßen, Lifetime and failure modes of plasma sprayed thermal barrier coatings in thermal gradient rig tests with simultaneous CMAS injection, Surf. Coatings Technol. 324 (2017) 36–47, https://doi.org/10.1016/j.surfcoat.2017.04.071.
[7] J. Chevalier, L. Gremillard, A.V. Virkar, D.R. Clarke, The tetragonal-monoclinic transformation in zirconia: lessons learned and future trends, J. Am. Ceram. Soc. 92 (2009) 1901–1920, https://doi.org/10.1111/j.1551-2916.2009.03278.x.
[8] N.I. Baklanova, B.A. Kolesov, T.M. Zima, Raman study of yttria-stabilized zirconia interfacial coatings on Nicalon™ fiber, J. Eur. Ceram. Soc. 27 (2007) 165–171, https://doi.org/10.1016/j.jeurceramsoc.2006.04.151.
[9] G. Witz, V. Shklover, W. Steurer, S. Bachegowda, H.P. Bossmann, Phase evolution in yttria-stabilized zirconia thermal barrier coatings studied by rietveld refinement of X-ray powder diffraction patterns, J. Am. Ceram. Soc. 90 (2007) 2935–2940, https://doi.org/10.1111/j.1551-2916.2007.01785.x.
[10] S. Sampath, U. Schulz, M.O. Jarligo, S. Kuroda, Processing science of advanced thermal-barrier systems, MRS Bull. 37 (2012) 903–910, https://doi.org/10.1557/mrs.2012.233.
[11] M.P. Borom, C.A. Johnson, L.A. Peluso, Role of environmental deposits and operating surface temperature in spallation of air plasma sprayed thermal barrier coatings, Surf. Coatings Technol. 86–87 (1996) 116–126, https://doi.org/10.1016/S0257-8972(96)02994-5.
[12] F.H. Stott, D.J. De Wet, R. Taylor, Degradation of thermal-barrier coatings at very high temperatures, MRS Bull. 19 (1994) 46–49, https://doi.org/10.1557/S0883769400048223.
[13] J.L. Smialek, F.A. Archer, R.G. Garlick, Turbine airfoil degradation in the persian gulf war, J. Miner. Met. Mater. Soc. 46 (1994) 39–41, https://doi.org/10.1007/BF03222663.
[14] P. Mechnich, W. Braue, U. Schulz, High-temperature corrosion of EB-PVD yttria partially stabilized zirconia thermal barrier coatings with an artificial volcanic ash overlay, J. Am. Ceram. Soc. 94 (2011) 925–931, https://doi.org/10.1111/j.1551-2916.2010.04166.x.

[15] R. Naraparaju, J.T. Gomez Chavez, U. Schulz, C.V. Ramana, Interaction and infiltration behavior of Eyjafjallajökull, Sakurajima volcanic ashes and a synthetic CMAS containing FeO with/in EB-PVD ZrO2-65 wt% Y2O3coating at high temperature, Acta Mater. 136 (2017) 164–180, https://doi.org/10.1016/j.actamat.2017.06.055.
[16] J.M. Drexler, A.D. Gledhill, K. Shinoda, A.L. Vasiliev, K.M. Reddy, S. Sampath, N.P. Padture, Jet engine coatings for resisting volcanic ash damage, Adv. Mater. 23 (2011) 2419–2424, https://doi.org/10.1002/adma.201004783.
[17] S. Krämer, J. Yang, C.G. Levi, C.A. Johnson, Thermochemical interaction of thermal barrier coatings with molten CaO-MgO-Al2O3-SiO2 (CMAS) deposits, J. Am. Ceram. Soc. 89 (2006) 3167–3175, https://doi.org/10.1111/j.1551-2916.2006.01209.x.
[18] R. Naraparaju, P. Mechnich, U. Schulz, G.C. Mondragon Rodriguez, The accelerating effect of CaSO4 within CMAS (CaO-MgO-Al2O3-SiO2) and its effect on the infiltration behavior in EB-PVD 7YSZ, J. Am. Ceram. Soc. 99 (2016) 1398–1403, https://doi.org/10.1111/jace.14077.
[19] R. Naraparaju, U. Schulz, P. Mechnich, P. Döbber, F. Seidel, Degradation study of 7wt.% yttria stabilised zirconia (7YSZ) thermal barrier coatings on aero-engine combustion chamber parts due to infiltration by different CaO-MgO-Al2O3-SiO2variants, Surf. Coatings Technol. 260 (2014) 73–81, https://doi.org/10.1016/j.surfcoat.2014.08.079.
[20] A.K. Rai, R.S. Bhattacharya, D.E. Wolfe, T.J. Eden, CMAS-resistant thermal barrier coatings (TBC), Int. J. Appl. Ceram. Technol. 7 (2010) 662–674, https://doi.org/10.1111/j.1744-7402.2009.02373.x.
[21] W. Braue, Environmental stability of the YSZ layer and the YSZ/TGO interface of an in-service EB-PVD coated high-pressure turbine blade, J. Mater. Sci. 44 (2009) 1664–1675, https://doi.org/10.1007/s10853-008-3215-8.
[22] J.M. Drexler, K. Shinoda, A.L. Ortiz, D. Li, A.L. Vasiliev, A.D. Gledhill, S. Sampath, N.P. Padture, Air-plasma-sprayed thermal barrier coatings that are resistant to high-temperature attack by glassy deposits, Acta Mater. 58 (2010) 6835–6844, https://doi.org/10.1016/j.actamat.2010.09.013.
[23] V.L. Wiesner, N.P. Bansal, Mechanical and thermal properties of calcium-magnesium aluminosilicate (CMAS) glass, J. Eur. Ceram. Soc. 35 (2015) 2907–2914, https://doi.org/10.1016/j.jeurceramsoc.2015.03.032.
[24] R. Bonasia, C. Scaini, L. Capra, M. Nathenson, C. Siebe, L. Arana-Salinas, A. Folch, Long-range hazard assessment of volcanic ash dispersal for a Plinian eruptive scenario at Popocatepetl volcano (Mexico): implications for civil aviation safety, Bull. Volcanol. 76 (2014) 1–16, https://doi.org/10.1007/s00445-013-0789-z.
[25] R. Saucedo, J.L. Macías, M.F. Sheridan, M.I. Bursik, J.C. Komorowski, Modeling of pyroclastic flows of Colima Volcano, Mexico: implications for hazard assessment, J. Volcanol. Geotherm. Res. 139 (2005) 103–115, https://doi.org/10.1016/j.jvolgeores.2004.06.019.
[26] D. Lozano-Mandujano, Fabricación de Recubrimientos para Barreras Térmicas de Materiales Base La2Zr2O7 Depositados Mediante APS, y Caracterización de sus Propiedades Mecánicas y Estructurales, Centro de Investigación y de Estudios Avanzados del IPN, 2014.
[27] A.G. Mora-García, H. Ruiz-Luna, M. Mosbacher, R. Popp, U. Schulz, U. Glatzel, J. Muñoz-Saldaña, Microstructural analysis of Ta-containing NiCoCrAlY bond coats deposited by HVOF on different Ni-based superalloys, Surf. Coatings Technol. 354 (2018) 214–225, https://doi.org/10.1016/j.surfcoat.2018.09.025.
[28] H. Toraya, M. Yoshimura, S. Somiya, Calibration curve for quantitative analysis of the monoclinic-tetragonal ZrO_2 system by X-ray diffraction, Commun. Am. Ceram. Soc. 67 (1984) C119–C121, https://doi.org/10.1111/j.1151-2916.1984.tb19715.x.
[29] W. Li, H. Zhao, X. Zhong, L. Wang, S. Tao, Air plasma-sprayed yttria and yttria-stabilized zirconia thermal barrier coatings subjected to calcium-magnesium-alumino-silicate (CMAS), J. Therm. Spray Technol. 23 (2014) 975–983, https://doi.org/10.1007/s11666-014-0107-0.
[30] C. Cai, S. Chang, Y. Zhou, L. Yang, G. Zhou, Y. Wang, Microstructure characteristics of EB-PVD YSZ thermal barrier coatings corroded by molten volcanic ash, Surf. Coatings Technol. 286 (2016) 49–56, https://doi.org/10.1016/j.surfcoat.2015.12.003.
[31] D. Giordano, J.K. Russell, D.B. Dingwell, Viscosity of magmatic liquids: a model, Earth Planet. Sci. Lett. 271 (2008) 123–134, https://doi.org/10.1016/j.epsl.2008.03.038.
[32] R.G. Kuryaeva, Degree of polymerization of aluminosilicate glasses and melts, Glas. Phys. Chem. 30 (2004) 157–166, https://doi.org/10.1023/B:GPAC.0000024000.19443.f6.
[33] W. Song, K. Hess, Y. Lavallée, U. Kueppers, C. Cimarelli, Volcanic Ash Melting in Jet Engines : A Criterion, (n.d.).
[34] W.R. Chen, L.R. Zhao, Review - volcanic ash and its influence on aircraft engine components, Procedia Eng 99 (2015) 795–803, https://doi.org/10.1016/j.proeng.2014.12.604.
[35] H. Zhao, C.G. Levi, H.N.G. Wadley, Molten silicate interactions with thermal barrier coatings, Surf. Coatings Technol. 251 (2014) 74–86, https://doi.org/10.1016/j.surfcoat.2014.04.007.
[36] J. Wu, H. bo Guo, Y. zhi Gao, S. kai Gong, Microstructure and thermo-physical properties of yttria stabilized zirconia coatings with CMAS deposits, J. Eur. Ceram. Soc. 31 (2011) 1881–1888, https://doi.org/10.1016/j.jeurceramsoc.2011.04.006.
[37] P. Mohan, T. Patterson, B. Yao, Y. Sohn, Degradation of thermal barrier coatings by fuel impurities and CMAS: thermochemical interactions and mitigation approaches, J. Therm. Spray Technol. 19 (2010) 156–167, https://doi.org/10.1007/s11666-009-9424-0.
[38] P. Mohan, B. Yuan, T. Patterson, V. Desai, Y.H. Sohn, Degradation of yttria stabilized zirconia thermal barrier coatings by molten CMAS ($CaO-MgO-Al_2O_3-SiO_2$) deposits, Mater. Sci. Forum 595–598 (2008) 207–212, https://doi.org/10.4028/www.scientific.net/msf.595-598.207.
[39] P. Mohan, B. Yuan, T. Patterson, V.H. Desai, Y.H. Sohn, Degradation of yttria-stabilized zirconia thermal barrier coatings by vanadium pentoxide, phosphorous pentoxide, and sodium sulfate, J. Am. Ceram. Soc. 90 (2007) 3601–3607, https://doi.org/10.1111/j.1551-2916.2007.01941.x.
[40] M. Craig, N.L. Ndamka, R.G. Wellman, J.R. Nicholls, CMAS degradation of EB-PVD TBCs: the effect of basicity, Surf. Coatings Technol. 270 (2015) 145–153, https://doi.org/10.1016/j.surfcoat.2015.03.009.
[41] A.R. Krause, B.S. Senturk, H.F. Garces, G. Dwivedi, A.L. Ortiz, S. Sampath, N.P. Padture, 2ZrO2·Y2O3thermal barrier coatings resistant to degradation by molten CMAS: part I, optical basicity considerations and processing, J. Am. Ceram. Soc. 97 (2014) 3943–3949, https://doi.org/10.1111/jace.13210.
[42] R. Naraparaju, J.J. Gomez Chavez, P. Niemeyer, K.U. Hess, W. Song, D.B. Dingwell, S. Lokachari, C.V. Ramana, U. Schulz, Estimation of CMAS infiltration depth in EB-PVD TBCs: a new constraint model supported with experimental approach, J. Eur. Ceram. Soc. 39 (2019) 2936–2945, https://doi.org/10.1016/j.jeurceramsoc.2019.02.040.
[43] U. Kueppers, C. Cimarelli, K.U. Hess, J. Taddeucci, F.B. Wadsworth, D.B. Dingwell, The thermal stability of Eyjafjallajökull ash versus turbine ingestion test sands, J. Appl. Volcanol. 3 (2014) 1–11, https://doi.org/10.1186/2191-5040-3-4.
[44] J.F. White, J. Lee, O. Hessling, B. Glaser, Reactions between liquid CaO-SiO2 slags and graphite substrates reactions between liquid CaO-SiO 2 slags and graphite substrates, Metall. Mater. Trans. B Process Metall. Mater. Process. Sci. (2016), https://doi.org/10.1007/s11663-016-0788-5.
[45] V.L. Wiesner, N.P. Bansal, Crystallization kinetics of calcium-magnesium aluminosilicate (CMAS) glass, Surf. Coatings Technol. 259 (2014) 608–615, https://doi.org/10.1016/j.surfcoat.2014.10.023.
[46] H.G. Huckenholz, Synthesis and stability of Ti-andradite, Am. J. Sci. 267 (1969) 209–232 http://earth.geology.yale.edu/~ajs/1969/ajs_267A_11.pdf/209.pdf.
[47] Y. Richet, Pascal, Bottinga, Anorthite, andesine, wollastonite, diopside, cordierite and pyrope: thermodynamics of melting, glass transitions, and properties of the amorphous phases, Earth Planet. Sci. Lett. 67 (1984) 415–432.